Nanoscale

Nanocomplex Made of Antimicrobial Metallo-Supramolecule And Model Biomembranes – Characterization and Enhanced Fluorescence

Journal:	*Nanoscale*
Manuscript ID	NR-ART-06-2021-004083.R1
Article Type:	Paper
Date Submitted by the Author:	23-Jul-2021
Complete List of Authors:	Liu, Chung-Hao; University of Connecticut, Polymer Program, Institute of Materials Science Wang, Heng; Shenzhen University, College of Chemistry and Environmental Engineering, Yang, Lin; Brookhaven National Laboratory, National Synchrotron Light Source Liu, Yun; National Institute of Standards and Technology, Center for Neutron Research, ; University of Delaware, Chemical Engineering Li, Xiaopeng; Shenzhen University, College of Chemistry and Environmental Engineering; University of South Florida, Department of Chemistry Nieh, Mu-Ping; University of Connecticut, Chemical and Biomolecular Engineering; University of Connecticut, Polymer Program, Institute of Materials Science

Nanocomplex Made of Antimicrobial Metallo-Supramolecule And Model Biomembranes – Characterization and Enhanced Fluorescence

*Chung-Hao Liu[a], Heng Wang[b], Lin Yang[c], Yun Liu[d,e], Xiaopeng Li[b], Mu-Ping Nieh[a,f]**

[a]Polymer Program, Institute of Material Science, University of Connecticut, Storrs, Connecticut 06269, United States

[b]College of Chemistry and Environmental Engineering, Shenzhen University, Shenzhen 518055, China

[c]National Synchrotron Light Source – II, Brookhaven National Laboratory, Upton, NY, United States

[d]Center for Neutron Research, National Institute of Standards and Technology, Gaithersburg, Maryland 20899, United States

[e]Chemical & Biomolecular Engineering Department, University of Delaware, Newark, Delaware 19716, United States

[f]Department of Chemical and Biomolecular Engineering, University of Connecticut, Storrs, Connecticut 06269, United States

Key words: Bicelle, self-assembly, supramolecule, nanocomplex, vSANS, SAXS, TEM, Aggregation enhanced emission

ABSTRACT

Antimicrobial pentatopic 2,2':6',2"-terpyridines that form 3-D supramolecular hexagonal prisms with Cd^{2+} through coordination driven self-assembly, can be entrapped by lipid discoidal bicelles, composed of 1,2-dipalmitoyl-sn-glycero-3-phosphocholine, 1,2-dihexanoyl-sn-glycero-3-phosphocholine and 1,2-dipalmitoyl-sn-glycero-3-phospho-(1'-rac-glycerol) lipid, forming a well-defined nanocomplex. Structural characterization performed by very small angle neutron scattering,

small angle X-ray scattering and transmission electron microscopy suggests that the hexagonal prisms preferably locate at the rim of bicellar discs with the hexagonal face in parallel with the bilayers, instead of face-to-face stacking. Such a configuration reduces the π–π interaction and consequently enhances the fluorescence emission. Since the novel supramolecule was reported to have antibiotic functions, this study provides the insight to the interactions of antimicrobial supermolecules with lipid membranes, leading to potential theranostic applications.

INTRODUCTION

Recently, rational design of novel 3-D supramolecules with well-defined cavities, constructed by coordination-driven self-assembly, have attracted substantial attention in the supramolecular fields. They provide great potential for developing desired supramolecules for many applications in sensing[1], optoelectronic devices[2], drug delivery[3], and artificial transmembrane channels[4]. A recently designed 3-D hexagonal prism (**HP**) synthesized by pentatopic 2,2':6',2"-terpyridine (P-TPY) with three different environments (Figure 1, TPY^{a-c})[5] shows potent antimicrobial activities against two Gram-positive bacteria, including MRSA and Bacillus subtilis (B. subtilis), leading to a potential solution for the emergent challenge of shortage of antibodies. However, the **HP** only dissolves in the organic solvents, i.e., acetone nitrate, methanol, or dimethyl sulfoxide (DMSO), which are not ideal candidates for biological use. To overcome the challenge of biocompatibility and to understand the interactions between the supramolecules and biomembranes are important for in vivo administration of **HP**. This report therefore focuses on structural characterization of a **HP**/lipid nanocomplex, which greatly enhances the aqueous solubility as well as provides insight to the interaction of **HP** with biomembranes.

In the past, biocompatible lipid systems showed capability of entrapping hydrophobic molecules. One example is the discoidal bicellar system[6-9], composed of long-chain (L) lipids, e.g., dipalmitoyl

phosphatidylcholine (DPPC, di-C_{16}PC) and dipalmitoyl phosphati-dylgylcerol (DPPG, di-C_{16}PG), and short-chain (S) lipids, e.g., dihexanoyl phosphatidylcholine (DHPC, di-C_6PC), with molar ratios in the range of $2 \leq [L]/[S] \leq 5$.[6] The formation mechanism of nanodiscs is attributed to the hydrophobic interaction, immiscibility between S and L lipids, appropriate molecular spontaneous curvatures (one planar and the other rim) and sufficient surface charged density.[6] Such nanodiscs generally yield uniform radii (10 ~ 15 nm) and bilayer thickness (~ 5 nm). Most intriguingly, they demonstrate 5-10 times enhancement of cellular uptake compared against the vesicles of the same chemical compositions.[7, 8] Hence, bicelles can be an ideal nanocarrier platform for **HP,** not only enhancing the solubility in biologically relevant aqueous solution but also increasing the endocytosis of **HP**.

From the transmission electron microscopy (TEM), and small angle scattering (SAS) data, we found that **HP** can be successfully encapsulated in bicelles around the rim. Another intriguing discovery is that enhancement of fluorescence emission intensity is observed as **HP** is loaded in bicelles compared with the free **HP** in organic solvent, showing aggregation enhanced emission (AEE) as reported recently.[10, 11]

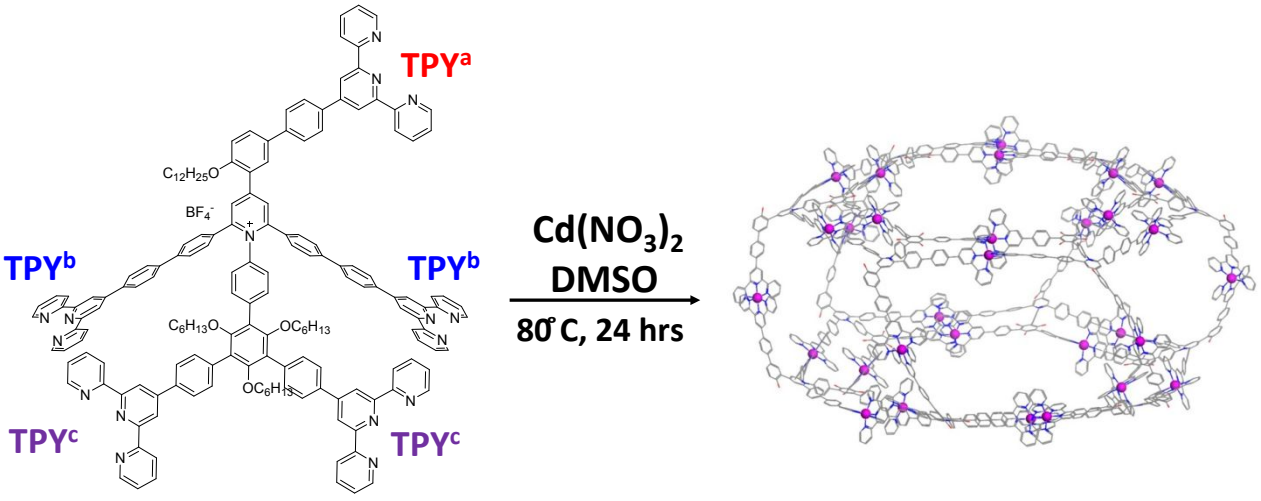

Figure 1. The 3-D chemical structure of **HP** self-assembly, where the alkyl chains are omitted for clarity.

RESULTS AND DISCUSSION

HP structure characterization. Figure 1 shows the proposed drum-like structure of **HP** self-assemblies through the designed coordination with Cd^{2+}. The dimensions of the **HP** self-assemblies in deuterated DMSO are characterized through best fitting the very small angle neutron scattering (vSANS) data with a core-shell cylinder model, as shown in Figure S4 and Table S1. The best fit yields a radius, a shell thickness and drum height of 2.3, 1.5 and 2.7 nm, respectively (supporting information) consistent with the previous report.[5] In order to encapsulate **HP** self-assemblies in lipid bilayer without imposing high stress to the biomembrane, at least one of the dimensions should be less than the bilayer thickness. The free **HP** self-assembly seems to satisfy the condition based on the structural characterization.

Encapsulation efficiency (EE). Since **HP** is practically insoluble in water, the preparation of **HP**-loaded bicelles (**HP-B**) was achieved by dispersed **HP** and lipids in $CHCl_3$ and methanol mixtures. The samples were then redispersed in water after dried. **HP** can be loaded in the lipid self-assemblies through the hydrophobic interaction. Centrifugation was applied to remove the non-encapsulated **HP**. yielding yellowish **HP-B**.

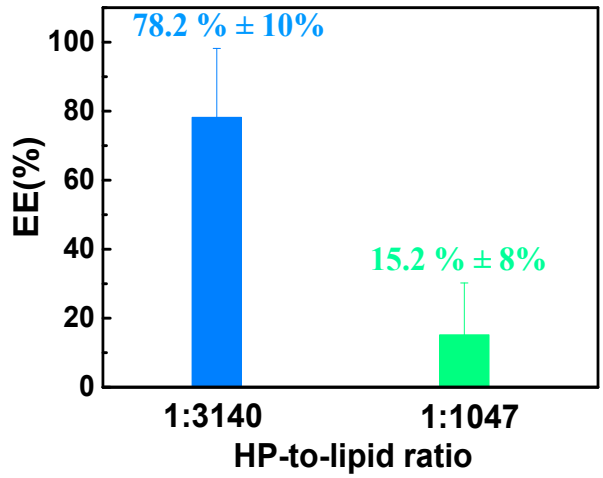

Figure 2. The EE% of samples with the **HP**-to-lipid ratios of 1:3140 and 1:1047, yielding the results of (78% ± 10%) and (15.2% ± 8 %), respectively.

The quantity of encapsulated **HP** can be determined from the pre-calibrated UV-vis absorption spectra where the absorption is linearly dependent on the concentration of **HP** (Figure S5). Figure 2 shows the EE% of the **HP**-to-lipid molar ratio of 1:3140 and 1:1470. The sample with **HP**-to-lipid ratio of 1:3140 has an EE% of 78% ± 10%, which drastically decreases to 15% ± 8% for the higher **HP**-to-lipid ratio (1:1047) sample due to the fact that the sample of high **HP**-to-lipid ratio destabilized the discoidal structure of nanocomplex into vesicles (Figure S6). Therefore, our analysis mainly focuses on the 1:3140 **HP-B**.

Absorption and emission spectrum. Figure 3(a) shows the UV-vis absorption of the pristine bicelles (**PB**), 1:3140 **HP-B** and free **HP**, respectively. The **PB** illustrate no absorbance in the probing range of wavelength. For comparison purpose, the absorption spectrum of **HP–B** is normalized according to EE%. The absorption spectra of **HP-B** (in aqueous solution) and free **HP** (in $CHCl_3$/MeOH) exhibit a maximum peak at 286 nm from the pentatopic TPY ligands (P-TPY). The absorption peak slightly shifts from 291 nm to 286 nm (Figure S7). The phenomenon is also observed when ligands coordinated with Zn(II)[12] and Cd(II)[13] to form metallo-supramolecules. The shoulder peak for free **HP** around 320 nm may result from $\pi \rightarrow \pi^*$ due to the supramolecular stacking (π-π interaction) [13, 14] of a tubular-like self-assembling structure of **HPs** in organic solvent.[5, 15] The reduced absorbance of 320 nm of the **HP-B** suggests weaker π-π interactions. [13, 14] As the **HP-B** was dried and redispersed into the mixture of $CHCl_3$/MeOH, the absorption spectrum was found identical with that of free **HP** (Figure S8) indicating the same drum-like structure of **HP**. It should be noted that drum-like **HP** only forms in organic solvent (e.g., DMSO) at 80 ^oC for 12 hours (Figure 1). The fact that the drying process and re-dispersion in $CHCl_3$/MeOH were conducted at 50 ^oC and room temperature, respectively suggests that it is unlikely for the **HP** to dissociate after encapsulation in the first place and then assemble into a drum-like structure again.

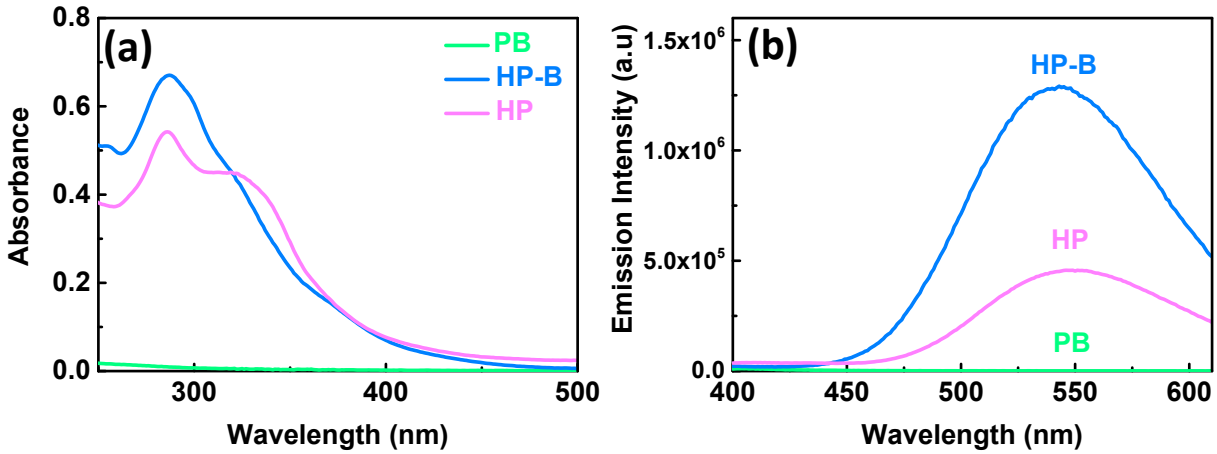

Figure 3. (a) The UV-vis absorption and (b) emission spectra (λ_{ex}= 320 nm) of **PB**, **HP-B** and **HP**.

The **HP** exhibits fluorescence with the maximum emission wavelength, λ_{em} of 550 nm (at λ_{ex}= 320 nm) as shown in Figure 3(b). Like most of the organic fluorophores, the normalized emission intensity of "free" **HP** decreases with increased **HP** concentrations (Figure S9).The highest normalized emission intensity was found at the lowest **HP** concentration, due to the aggregation-caused quench (ACQ) effect, presumably due to the preferably base-to-base self-assembly by π-π interactions. [5,16, 17]Intriguingly, the **HP-B** (1:3140) emits a three-fold intensity compared to the free **HP** solution at the same concentration [Figure 3(b)]. However, 1:1047 **HP-B** shows less emission (Figure S10) due to either low EE% or morphological disruption (Figure S6). The emission peak slightly shifts from 550 nm to 543 nm [Fig. 3(b)] possibly because of less π-π interactions in **HP-B** as π-π interaction is expectedly leading to the red shift of fluorescence.[18-20] The emission enhancement in conjunction with the blue shift suggest reduced base-to-base configuration. Another possible explanation would be the restricted intramolecular motion (RIM) as **HP** is confined in the bicelles causing the so-called aggregation-enhanced emission (AEE).[10, 20] Most importantly, the different emission spectra between **HP-B** and metal-free P-TPYas shown in Figure 4 suggests that the **HP** likely retains the 3D drum-like structure after encapsulation.

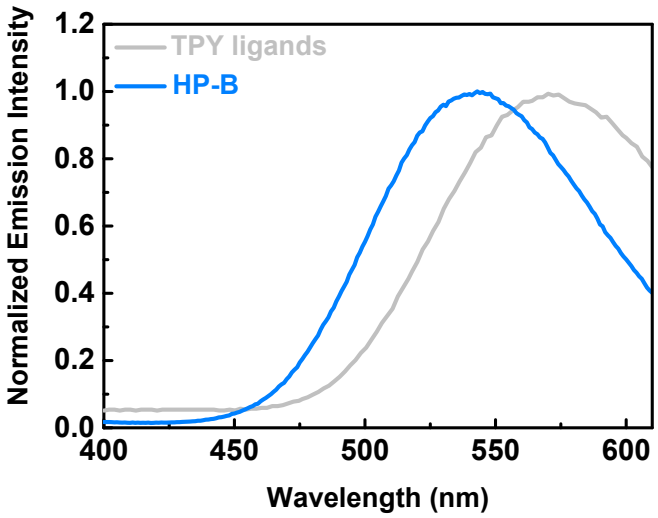

Figure 4. The fluorescence spectra of pentatopic TPY ligands (λ_{ex}= 280 nm), and **HP-B** (λ_{ex}= 320 nm). The intensity is normalized by peak intensity for clarity of the peak position.

Structural Characterization of the HP-B. The morphology of **HP-B** and location of **HP** in the bicelles reveal the interactions between **HP** and lipids. Both TEM micrographs of **PB** and **HP-B** indicate that nanodiscs retains regardless of the encapsulation of **HP**. However, the **PB** are overall smaller with an average diameter of ~ 16.8 (± 4.5 nm) [Figure 5(a) and 5(b)], consistent with the literature values,[6] while the **HP-B** yields larger discs with an average diameter of 30.6 (± 7.8 nm) [Figure 5(d) and 5(e)]. The darker rim of **HP-B** [Figure 5(c) and 5(f)] implies that the encapsulated **HP** (with higher electron density) may preferably locate at the rim of bicelles. The internal structure of **HP-B** can be revealed by vSANS using the DPPG, deuterated DPPC-d_{62} and DHPC-d_{35} with the average neutron scattering length density (NSLD), ρ_{lipid} of 5.12 × 10^{-6} Å^{-2} in a null-contrast solvent at D_2O/H_2O = 82/18, where $\rho_{solvent}$ equals ρ_{lipid}.[21] The contrast between the protiated **HP** and the rest components is therefore enhanced as shown in Figure S11. As the vSANS data (Figure S12) can be fitted by a core-shell discoidal model (CSD, Figure S2), the best fitting parameters (Table S2) show a decreased rim NSLD presumably due to the lower NSLD of protiated **HP**, indicating that **HP**s preferably situate themselves at the rim, in good agreement with the TEM

results. Furthermore, the hydrophobic thickness (L_{length}) of the bicellar planar region is in the range between 37 Å and 39 Å (Table S2) with minimal dependence of **HP**-loading, suggesting that **HP** is unlikely inserted in the bilayer.

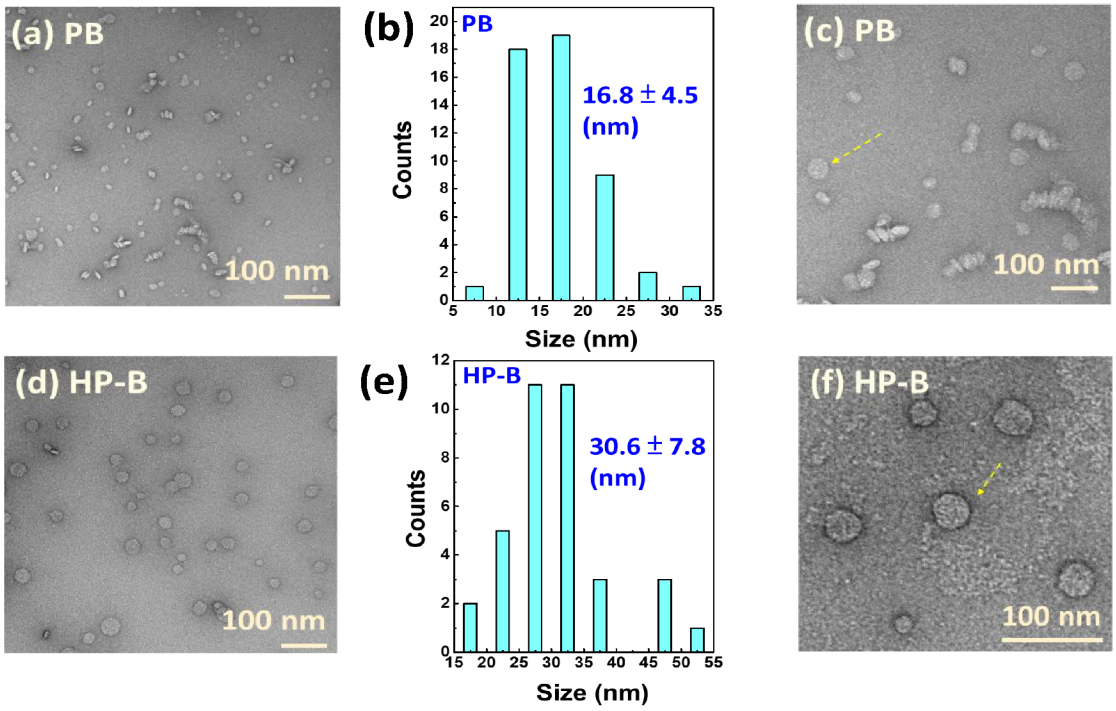

Figure 5. (a), (c) and (d), (f) are TEM images of **PB** and **HP-B**, respectively, on the same copper grids b different locations. (b) and (e) are the diameter distribution which is obtained from Image J. The yellow arrows show higher electron densities of the rim of the **HP-B** in comparison with that of the **PB**.

SAXS can also provide structural information of **HP-B** as the phosphate groups of lipids and the middle of the bilayer, respectively, have the highest and lowest electron density across the bilayer, rendering three significant broad peaks in the range of scattering vector, q between 0.05 and 0.5 Å^{-1}. A five-layer core shell discoidal model (5LCSD), instead of CSD model, was used to fit the SAXS data to reveal the detailed internal bilayer structure with the lengths and electron densities of methylene and methyl regimes [Figure 6(a)].[22] Figure 6 (b) shows the reduced SAXS data and

their best fits. The Hayter-Penfold model (structure factor), which is commonly used for describing interparticle Coulombic repulsion, is required for interpreting the low-q intensity with a peak at ~ 0.015 Å^{-1} for **PB**, while no structure factor is required for **HP-B** presumably due to larger interparticle spacing with lager discs. Two of the high-q peaks at 0.27 Å^{-1} and 0.405 Å^{-1} slightly move to 0.28 Å^{-1} and 0.425 Å^{-1}, respectively, after loading of the **HP** [Figure 6(c)] indicates subtle structural changes. The best fitting radius of **HP-B** increases from 83 (±1) Å to 306 (±10) Å and the rim thickness, T_r, [Figure 6(a)] also increases from (47 ± 27) Å to (208 ± 7) Å, agreeing with the TEM and vSANS analyses which show the entrapped **HP** preferably located at the rim, leading to a larger T_r. The outcome is consistent with a previous report of hydrophobic gold nanoclusters entrapped at the bicellar rim, which is mainly made of fluidic DHPC in the L_α phase.[23-25]

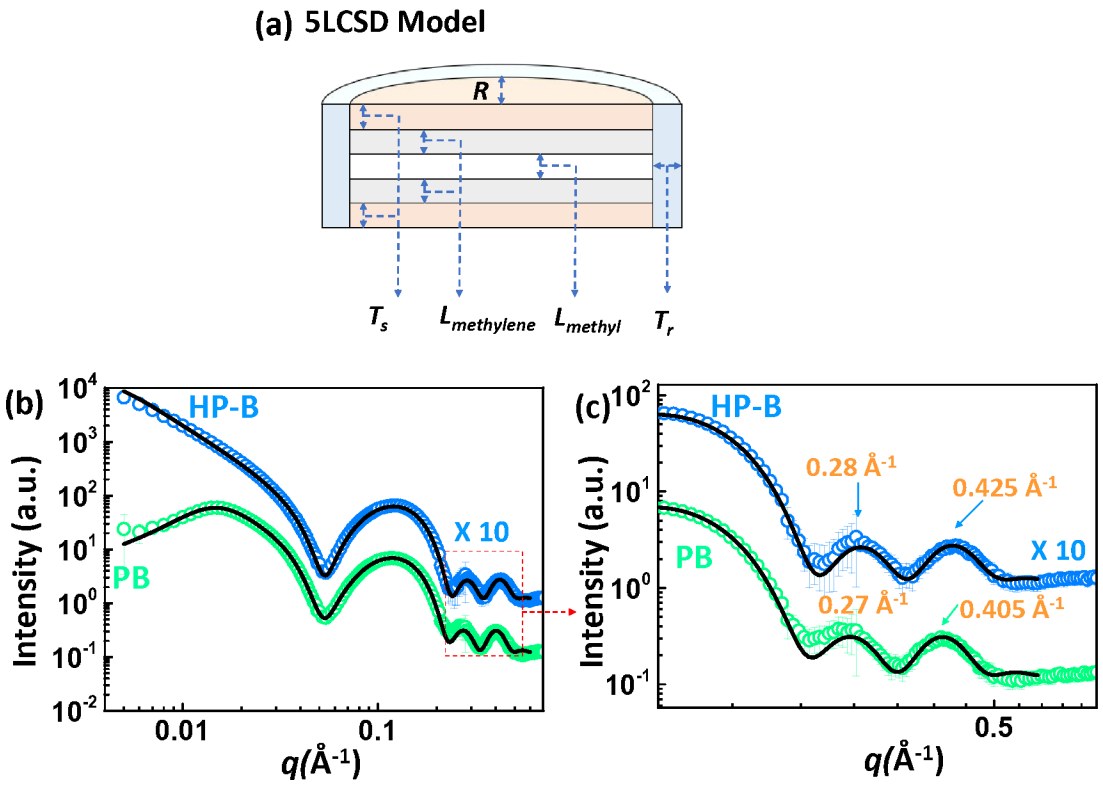

Figure 6. (a) The cross-section of 5LCSD model. (b) 1-D SAXS results of **PB** (blue) and **HP-B** (green). (c) The blowup of the dashed box in (b) with a zoomed-in view. The data of **HP-B** is scaled by 10 for clarity.

Table 1. The best fitted results of **PB** and **HP**-B

Parameters /Samples	**PB**	**HP-B**
Core radius (Å)	83 ± 1	319 ± 11
T_r *(Å)*	47 ± 27	204 ± 6
$L_{methylene}$ *(Å)*	13 ± 0.2	12 ± 0.3
L_{methyl} *(Å)*	11 ± 0.5	9 ± 0.6
$\rho_{methylene}$ $(10^{-6}/Å^2)$	9.47 ± 0.01	9.47 ± 0.01
ρ_{methyl} $(10^{-6}/Å^2)$	8.76 ± 0.02	8.72 ± 0.03
ρ_{rim} $(10^{-6}/Å^2)$	9.47 ± 0.01	9.50 ± 0.01

Thermal analysis of HP-B. Figure 7(a) and (b) show the DSC thermograms of **PB** and 1:3140 **HP-B** with 0.1 wt.% of lipid concentration. For **PB** [Fig. 7(a)], the peaks at 41 and 45 C correspond to the melting transition temperature (T_m) of DPPC and bicelle-to-vesicle transformation, respectively.[26] The identical thermogram on the second-time *T*-scan suggests reversibility of the bicelle-to-vesicle structural transformation of **PB** in contrast to the previous reports, which show irreversibility of the structural transformation after the 2nd thermal cycles,[26-28] The main reason is that the applied higher charge density (R=0.05) of **PB** stabilizes the discoidal structure.[21] The DSC thermograms of **HP-B**, however, show irreversibility of the bicelle-to-vesicle transformation after the first thermal cycling, similar to the irreversible behavior in the weakly charged systems, where high-*T* vesicle retains after being cooled down. We thus hypothesize that the entrapment of **HP** destabilizes the discoidal morphology. Another interesting observation is that the enthalpy to melt gel-DPPC (area underneath the 41 C peak) of the **HP-B** is found significantly higher than that of **PB**. This suggests that more DHPC is driven to the rim to shield **HP**, resulting in greater segregation between DPPC and DHPC, yielding higher quantity of gel phase and consequently larger discs, consistent with the TEM and SAXS outcomes.

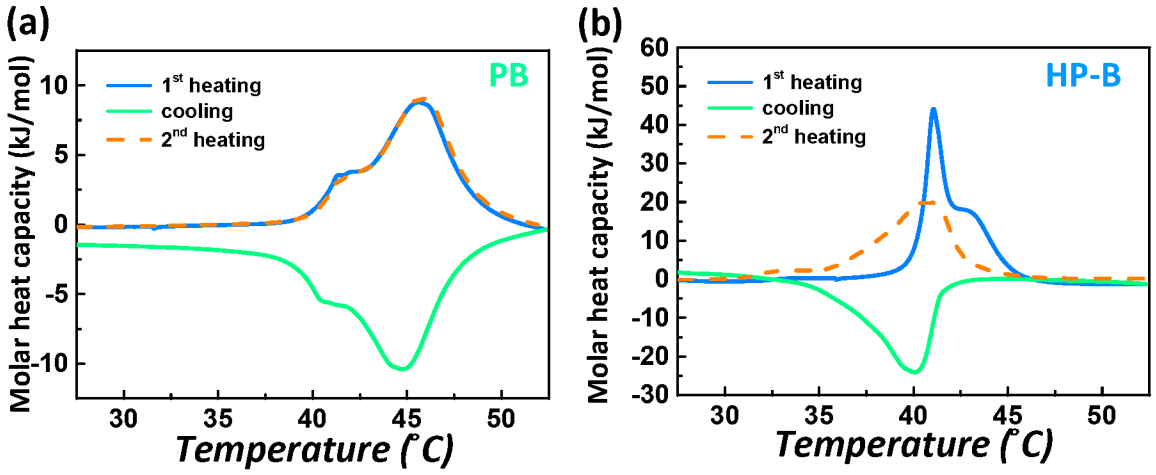

Figure 7. DSC thermograms of (a) the **PB** and (b) the **HP-B** undergoing a heating-cooling-heating process.

The previous report revealed that the **HP** adopted the base-to-base stacking [Fig. 8(a)] in organic solvent.[5] Since the diameters of the **HP** "drum" is found 7.6 nm, larger than two-fold of the bilayer hydrophobic thickness (~ 3.7 nm). It is not feasible to maintain the same aggregation behavior in the bicelles but takes less energy when the hexagonal face of the **HP** orients parallel with the bilayer as shown in Fig. 8(b). Such molecular arrangement reduces the π-π interaction, which agrees well with the observation of blue-shifted fluorescence spectra and consequently shows the enhancement in emission as described previously.

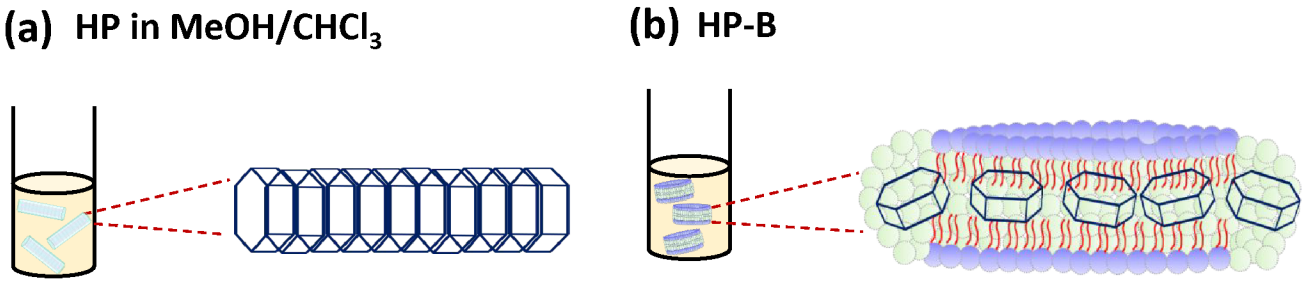

Figure 8. The schematics of (a) the stacking **HP** in the organic solvent and (b) a **HP-B**.

CONCLUSIONS

We have confirmed that the hydrophobic drum-like self-assembled supramolecule, **HP**, can be encapsulated in uniform-sized discoidal bicelles forming a well-defined nanoframe-in-nanodisc complex. Such one-pot synthesis with high E.E. (~75%) greatly enhances the concentration of **HP** dispersed in aqueous solutions. All experimental evidences suggest that **HP** preferable locates at the high-curvature rim made of the DHPC, allowing interaction with hydrophobic molecules.[24, 25, 29] Moreover, the **HP-B** exhibit three-fold emission intensity compared with that of the free **HP** in the organic solvent, presumably because the entrapped **HP** self-assemblies reduce the base-to-base stacking. Instead, they may be packed at the rim parallel with the bilayer. The UV-vis and fluorescence spectra show that the **HP** likely maintains drum shape in the interior of the bicelles.

The **HP-B** platform further increases the biocompatibility and solubility in aqueous solution, enabling its antimicrobial function more applicable for in vivo study. The enhancement of emission also makes it a potential candidate for theranostic purpose. Furthermore, this study further provides insight into understanding the structure-function relationship of supramolecules interacting with biomembranes.

AUTHOR CONTRIBUTIONS

C.-H. L., performed the experiments, analyzed data, and wrote the manuscript. H. W. and X. Li. designed and synthesized the supramolecule, **HP**. L. Y. and Y. L. are the beam time scientists at Brookhaven National Lab and National Institute of Standards and Technology. M.-P. N. supervised the entire project. All authors reviewed, edited and approved the manuscript prior to submission.

CONFLICTS OF INTEREST

The authors declare no conflicts of interest.

ACKNOWLEDGMENTS

The authors thank to the beamtime of 16ID-LiX at the NSLS-II (Brookhaven National Lab) through a beamtime proposal (BAG-302208). The LiX beamline is part of the Life Science Biomedical Technology Research resource, jointly supported by the National Institute of Health, National Institute of General Medical Sciences under Grant P41 GM111244, and by the Department of Energy Office of Biological and Environmental Research under Grant KP1605010, with additional support from NIH Grant S10OD012331. NSLS-II is a U.S. Department of Energy (DOE) Office of Science User Facility operated for the DOE Office of Science by Brookhaven National Laboratory under Contract No. DE-SC0012704. Access to vSANS was provided by the Center for High Resolution Neutron Scattering, a partnership between the National Institute of Standards and Technology and the National Science Foundation under Agreement No. DMR-2010792.

DISCLAIM

Access to vSANS was provided by the Center for High Resolution Neutron Scattering, a partnership between the National Institute of Standards and Technology and the National Science Foundation under Agreement No. DMR-2010792. Certain commercial equipment, instruments, or materials (or suppliers, or software...) are identified in this paper to foster understanding. Such identification does not imply recommendation or endorsement by the National Institute of Standards and Technology, nor does it imply that the materials or equipment identified are necessarily the best available for the purpose.

REFERENCE

1. L. E. Kreno, K. Leong, O. K. Farha, M. Allendorf, R. P. Van Duyne and J. T. Hupp, *Chemical Reviews*, 2012, **112**, 1105-1125.
2. C. Wang, D. Liu and W. Lin, *Journal of the American Chemical Society*, 2013, **135**, 13222-13234.
3. Y.-R. Zheng, K. Suntharalingam, T. C. Johnstone and S. J. Lippard, *Chemical Science*, 2015, **6**, 1189-1193.
4. C. J. E. Haynes, J. Zhu, C. Chimerel, S. Hernández-Ainsa, I. A. Riddell, T. K. Ronson, U. F. Keyser and J. R. Nitschke, *Angewandte Chemie International Edition*, 2017, **56**, 15388-15392.

5. H. Wang, C.-H. Liu, K. Wang, M. Wang, H. Yu, S. Kandapal, R. Brzozowski, B. Xu, M. Wang, S. Lu, X.-Q. Hao, P. Eswara, M.-P. Nieh, J. Cai and X. Li, *Journal of the American Chemical Society*, 2019, **141**, 16108-16116.
6. Y. Liu, Y. Xia, A. T. Rad, W. Aresh and M.-P. Nieh, in *Liposomes: Methods and Protocols*, ed. G. G. M. D'Souza, Springer New York, New York, NY, 2017, DOI: 10.1007/978-1-4939-6591-5_22, pp. 273-282.
7. W. Aresh, Y. Liu, J. Sine, D. Thayer, A. Puri, Y. Huang, Y. Wang and M. P. Nieh, *Journal of biomedical nanotechnology*, 2016, **12**, 1852-1863.
8. A. Tahmasbi Rad, C. W. Chen, W. Aresh, Y. Xia, P. S. Lai and M. P. Nieh, *ACS Appl Mater Interfaces*, 2019, **11**, 10505-10519.
9. A. Tahmasbi Rad, S. Malik, L. Yang, T. K. Oberoi-Khanuja, M.-P. Nieh and R. Bahal, *Nanoscale*, 2019, **11**, 12517-12529.
10. J. Luo, Z. Xie, J. W. Y. Lam, L. Cheng, H. Chen, C. Qiu, H. S. Kwok, X. Zhan, Y. Liu, D. Zhu and B. Z. Tang, *Chemical Communications*, 2001, DOI: 10.1039/B105159H, 1740-1741.
11. B. Z. Tang, X. Zhan, G. Yu, P. P. Sze Lee, Y. Liu and D. Zhu, *Journal of Materials Chemistry*, 2001, **11**, 2974-2978.
12. P. Narea, J. Cisterna, A. Cárdenas, P. Amo-Ochoa, F. Zamora, C. Climent, P. Alemany, S. Conejeros, J. Llanos and I. Brito, *Polymers*, 2020, **12**, 1756.
13. H. Wang, X. Qian, K. Wang, M. Su, W.-W. Haoyang, X. Jiang, R. Brzozowski, M. Wang, X. Gao, Y. Li, B. Xu, P. Eswara, X.-Q. Hao, W. Gong, J.-L. Hou, J. Cai and X. Li, *Nature Communications*, 2018, **9**, 1815.
14. J. Hermann, D. Alfè and A. Tkatchenko, *Nature Communications*, 2017, **8**, 14052.
15. C. Wei, Y. He, X. Shi and Z. Song, *Coordination Chemistry Reviews*, 2019, **385**, 1-19.
16. G.-Q. Yin, H. Wang, X.-Q. Wang, B. Song, L.-J. Chen, L. Wang, X.-Q. Hao, H.-B. Yang and X. Li, *Nature Communications*, 2018, **9**, 567.
17. J. Mei, Y. Hong, J. W. Y. Lam, A. Qin, Y. Tang and B. Z. Tang, *Advanced Materials*, 2014, **26**, 5429-5479.
18. X. Cao, L. Meng, Z. Li, Y. Mao, H. Lan, L. Chen, Y. Fan and T. Yi, *Langmuir*, 2014, **30**, 11753-11760.
19. X. Cao, Y. Li, A. Gao, Y. Yu, Q. Zhou, X. Chang and X. Hei, *Journal of Materials Chemistry C*, 2019, **7**, 10589-10597.
20. J. Li, J. Wang, H. Li, N. Song, D. Wang and B. Z. Tang, *Chemical Society Reviews*, 2020, **49**, 1144-1172.
21. M.-P. Nieh, C. J. Glinka, S. Krueger, R. S. Prosser and J. Katsaras, *Biophysical Journal*, 2002, **82**, 2487-2498.
22. C. Cheu, L. Yang and M.-P. Nieh, *Chemistry and Physics of Lipids*, 2020, **231**, 104945.
23. M. Kranenburg and B. Smit, *The Journal of Physical Chemistry B*, 2005, **109**, 6553-6563.
24. H. Sharma and E. E. Dormidontova, *ACS Nano*, 2017, **11**, 3651-3661.

25. A. T. Rad, Y. Bao, H.-S. Jang, Y. Xia, H. Sharma, E. E. Dormidontova, J. Zhao, J. Arora, V. John, B. Tang, T. Dainese, A. Hariri, J. Jokerst, F. Maran and M.-P. Nieh, *Advanced Functional Materials*, 2020, 2009750.
26. D. H. Ibtihal Alahmadi, Jr., Armin Tahmasbi Rad, Sanyukta Patil, Anas Alahmadi, Mu-Ping Nieh, *Langmuir*, 2021.
27. M.-P. Nieh, V. A. Raghunathan, S. R. Kline, T. A. Harroun, C.-Y. Huang, J. Pencer and J. Katsaras, *Langmuir*, 2005, **21**, 6656-6661.
28. M.-P. Nieh, P. Dolinar, N. Kučerka, S. R. Kline, L. M. Debeer-Schmitt, K. C. Littrell and J. Katsaras, *Langmuir*, 2011, **27**, 14308-14316.
29. Y. Xia, H.-S. Jang, Z. Shen, G. D. Bothun, Y. Li and M.-P. Nieh, *Langmuir*, 2017, **33**, 5745-5751.